Original Article

Journal of LOW FREQUENCY NOISE, VIBRATION AND ACTIVE CONTROL

Journal of Low Frequency Noise, Vibration and Active Control
2018, Vol. 37(4) 774–788

DOI: 10.1177/1461348418769779
journals.sagepub.com/home/lfn
SAGE

Nonlinear dynamical behaviors of a moving membrane under external excitation

Mingyue Shao[1], Jimei Wu[1,2], Yan Wang[3] and Shudi Ying[1]

Abstract

In this paper, the nonlinear vibration characteristics of a moving printing membrane under external excitation are studied. Based on the Von Karman nonlinear plate theory, the nonlinear vibration equation of the axial motion membrane under the external excitation is deduced. The Galerkin's method is used to discretize the vibration differential equations of the membrane, and then the state equation of the system is obtained. The state equation of the system is numerically solved by the fourth-order Runge–Kutta method. The relationship between the nonlinear vibration characteristics and the amplitude of external excitation, damping coefficient, and aspect ratio of the printing membrane is analyzed by using the time histories, phase-plane portraits, Poincare maps, and bifurcation diagrams. Chaotic intervals and the stable working range of the moving membrane are obtained. This study provides a theoretical basis for predicting and controlling the stability of the membrane.

Keywords

Nonlinear vibration, external excitation, moving membrane, fourth-order Runge–Kutta method

Introduction

The membrane, including plastic film, paper web, cloth, metal foil and other types of film-like material, is widely used in the manufacture of printing and packaging products. In the process of gravure printing, the printing membrane is subjected to a certain external excitation during printing or transmission, i.e. during the printing process, there is a printing pressure when the ink is transferred to the surface of the membrane. During the transfer process, the membrane is affected by the impact of the hot air in the oven, so the nonlinear vibration characteristics of the high-speed printing membrane will change, thereby the membrane instability phenomenon such as wrinkling, tearing, and surface scratches can be caused by the transverse vibrations of the membrane under external excitation, so the overprint accuracy and quality of printing are deteriorated.

In recent years, many scholars have studied more about the nonlinear vibration problem of the axial system, for example, strings, beams, plates, and so on but have less research on the nonlinear vibration characteristics of a membrane under external excitation.

Chen et al.[1] analyzed the steady-state periodic transverse responses and stabilities of axially accelerating viscoelastic strings. The amplitude, the existence conditions, and the stability were determined, and the effects of the viscosity, the mean axial speed, the axial speed fluctuation amplitude, and the axial support rigidity on the amplitude and the existence were examined via the numerical examples. Kesimli et al.[2] investigated the nonlinear

[1]School of Mechanical and Precision Instrument Engineering, Xi'an University of Technology, Xi'an, China
[2]Faculty of Printing, Packing and Digital Media Engineering, Xi'an University of Technology, Xi'an, China
[3]School of Civil Engineering and Architecture, Xi'an University of Technology, Xi'an, China

Corresponding author:
Jimei Wu, School of Mechanical and Precision Instrument Engineering, Xi'an University of Technology, Xi'an 710048, China.
Email: wujimei1@163.com

vibration characteristics of multi-supported axially moving string and the variable speed by multi-time-scaled method. Lewandowski and Wielentejczyk[3] applied the finite element method together with the harmonic balance method to study nonlinear vibration of beams under harmonic forces. Zenkour[4] analyzed the effect of length-to-thickness ratio and elastic foundation parameters on the natural frequencies of a thermoelastic microbeam resonator. Hadj et al.[5] employed the higher order shear deformation theories to obtain general differential equations of motion in nonlinear forced vibration analysis of multilayered composite beams. The equation of motion was obtained via Hamilton's principle and discretized by the Galerkin's method. Bifurcation diagrams of Poincare maps were obtained. Beni et al.[6] analyzed free vibration behavior of a single-walled carbon nanotube based on couple stress theory. Liu et al.[7] applied an optimal delayed feedback control method to mitigate the nonlinear vibration of a flexible simply–simply supported beam. Hirwani et al.[8] investigated transient responses of the shear deformable layered composite plate under the mechanical transverse (uniform and sinusoidal) loading by using the nonlinear finite element method. Kumar et al.[9] studied the nonlinear bending and vibration analyses of trapezoidal and arbitrary straight-sided quadrilateral composite plates by using smoothed finite element technique. Chai et al.[10] investigated the nonlinear dynamical analysis and design of the composite laminated plate with time-dependent boundary conditions based on the Von Karman plate theory and Bubnov Galerkin's method. Ghayesh et al.[11] applied Von Karman plate theory to examine the nonlinear vibration for forced motions of an axially moving plate, and the equations of motion were obtained via an energy method based on Lagrange equations. Khanna and Kaur[12] analyzed vibration characteristics of temperature-thickness coupling problem of a non-homogeneous isotropic viscoelastic rectangular plate. A numerical and an experimental study on optimal velocity feedback control for vibration suppression of a plate-like structure by Boz, Aridogan and Basdogan,[13] and the results showed that the developed control methodology effectively suppressed the vibration amplitudes at multiple modes of the structure. The improved multiple-scale method was used to analyze the nonlinear vibration and chaotic motion of the axially moving current-conducting thin plate under external harmonic force in magnetic field by Hu and Zhang.[14] Ansari et al.[15] studied the nonlinear mechanical behavior of plates based on the micropolar elasticity theory. Saleema and Manoranjan[16] investigated the nonlinear free flexural vibration of stiffened plates by using a super parametric element. Khanna and Singhal[17] studied vibration of isotropic tapered rectangular plate with different boundary conditions by using Rayleigh Ritz technique. Wang and Zu applied[18] the method of harmonic balance and an adaptive step-size fourth-order Runge–Kutta technique to analyze nonlinear dynamic thermoelastic response of rectangular functionally graded material (FGM) plates with longitudinal velocity. Lin and Mote[19] established the nonlinear vibration of an axially moving web with small flexural stiffness under transverse loading by Von Karman nonlinear plate theory. The finite element method was applied to analyze nonlinear vibration of an axially moving membrane by Koivurova and Pramila.[20] Kulachenko et al.[21,22] used the finite element method to investigate nonlinear vibration and stability of the web. The Von Karman nonlinear plate theory and the differential quadrature method were employed to study the nonlinear vibration of the moving rectangular membrane by Zhao and Wang.[23] Soares and Gonçalves[24] investigated the nonlinear vibrations and instabilities of a stretched hyperelastic membrane by using the finite element method. Marynowski[25] studied nonlinear vibrations of beam-like model of two-dimensional axially moving web with time-dependent tension by using the Galerkin's method and the fourth-order Runge–Kutta method. The effects of the transport speed, the tension perturbation amplitude and the internal damping on the dynamic behavior of the system were numerically investigated. A fundamental theory for deformable webs not resisting any compressive membrane forces was developed through a direct derivation on the deformed configuration by Luo.[26] Nguyen and Hong[27] presented a control algorithm for suppression of the transverse vibration of an axially moving web system via regulation of axial velocity. Banichuk et al.[28] analyzed the dynamics and stability of a moving web under non-homogeneous tension by using analytical approaches. The natural frequencies of a specially orthotropic rectangular membrane were examined with respect to its design parameters by Wetherhold and Padliya.[29] A method was presented for inferring the initial tensions from measured vibration frequencies and the sensitivity of the tensions with respect to imprecision in the measured frequencies was demonstrated. Li et al.[30] investigated the stochastic dynamic response and reliability analysis of membrane structure under impact load by using perturbation method. Ma et al.[31] studied transverse vibration and instability of axially travelling web subjected to non-homogeneous tension, the influence of tension inhomogeneity on the critical velocity and mode shape was discussed.

Through the above literature survey, there are few studies on the nonlinear vibration of an axially moving rectangular membrane under external excitation. In this study, the nonlinear vibration characteristics of an axially moving

membrane under external excitation are studied by using the fourth-order Runge–Kutta method. The influence of the amplitude of external excitation, aspect ratio, and damping coefficient on the nonlinear vibration characteristics are analyzed by using the time histories, phase-plane portraits, Poincare maps, and bifurcation diagrams.

The model of the moving membrane under external excitation

Figure 1 shows the kinematic model of the axially moving rectangular membrane under external excitation. The membrane is soft and homogeneous and has no flexural stiffness, shear force, or bending moment. v_x is the velocity of the moving membrane in the x direction, a and b are the length and width of the membrane, separately. ρ is mass per unit area of the membrane, h denotes the thickness of the membrane, $P\cos\varpi t$ denotes in-plane uniform external excitation, and $w(x, y, t)$ denotes the transverse vibration displacement of web in z direction.

The velocity of the moving membrane in the transverse deflection $w(x, y, t)$ direction is

$$v_z(t) = \frac{dw(x, y, t)}{dt} = \frac{\partial w}{\partial t} + v_x \frac{\partial w}{\partial x} \tag{1}$$

The lateral acceleration of the moving membrane is obtained

$$a_z = \frac{dv_z(t)}{dt} = \frac{d\left(\frac{\partial w}{\partial t} + v_x \frac{\partial w}{\partial x}\right)}{dt} = \frac{\partial^2 w}{\partial t^2} + 2v_x \frac{\partial^2 w}{\partial x \partial t} + {v_x}^2 \frac{\partial^2 w}{\partial x^2} \tag{2}$$

The nonlinear vibration equations of the moving membrane are obtained based on the Von Karman nonlinear plate theory[32]

$$\rho\left(\frac{\partial^2 w}{\partial t^2} + 2v_x \frac{\partial^2 w}{\partial x \partial t} + {v_x}^2 \frac{\partial^2 w}{\partial x^2}\right) - N_x \frac{\partial^2 w}{\partial x^2} - N_y \frac{\partial^2 w}{\partial y^2} - 2N_{xy} \frac{\partial^2 w}{\partial x \partial y} - P\cos\varpi t = 0 \tag{3}$$

$$\frac{\partial^2 N_x}{\partial y^2} + \frac{\partial^2 N_y}{\partial x^2} - \lambda \frac{\partial^2 N_x}{\partial x^2} - \lambda \frac{\partial^2 N_y}{\partial y^2} = Eh\left[\left(\frac{\partial^2 w}{\partial x \partial y}\right) - \frac{\partial^2 w}{\partial x^2} \frac{\partial^2 w}{\partial y^2}\right] \tag{4}$$

where E is the modulus of elasticity and λ is the Poisson's ratio.

The internal force function of the membrane $\Phi(x, y)$ is introduced for equations (3) and (4)

$$\begin{cases} N_x = \dfrac{\partial^2 \Phi}{\partial y^2} \\ N_y = \dfrac{\partial^2 \Phi}{\partial x^2} \\ N_{xy} = -\dfrac{\partial^2 \Phi}{\partial x \partial y} \end{cases} \tag{5}$$

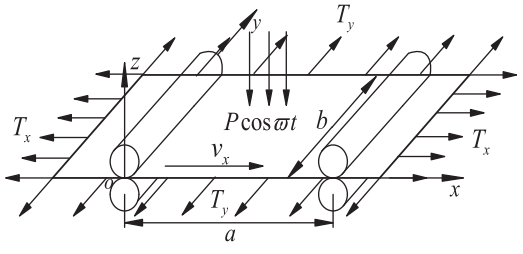

Figure 1. Mechanical model of the axial motion membrane under external excitation.

Because $N_{xy} = -\frac{\partial^2 \Phi}{\partial x \partial y} = 0$, so we can get

$$\frac{\partial}{\partial x \partial y}\left(\frac{\partial^2 \Phi}{\partial x \partial y}\right) = \frac{\partial^4 \Phi}{\partial x^2 \partial y^2} = 0 \tag{6}$$

Substituting equations (5) and (6) into equations (3) and (4) yields

$$\rho\left(\frac{\partial^2 w}{\partial t^2} + 2v_x \frac{\partial^2 w}{\partial x \partial t} + {v_x}^2 \frac{\partial^2 w}{\partial x^2}\right) - \frac{\partial^2 \Phi}{\partial y^2}\frac{\partial^2 w}{\partial x^2} - \frac{\partial^2 \Phi}{\partial x^2}\frac{\partial^2 w}{\partial y^2} - P\cos\varpi t = 0 \tag{7}$$

$$\frac{\partial^4 \Phi}{\partial x^4} + \frac{\partial^4 \Phi}{\partial y^4} = Eh\left[\left(\frac{\partial^2 w}{\partial x \partial y}\right)^2 - \frac{\partial^2 w}{\partial x^2}\frac{\partial^2 w}{\partial y^2}\right] \tag{8}$$

In order to make the research results more widely applicable to engineering problems of the moving membrane, the dimensionless quantities are adopted in solving the nonlinear vibration equation of the system and investigating the relationship between nonlinear vibration characteristics and various parameters. Introduce the dimensionless quantities

$$\begin{gathered} \varsigma = \frac{x}{a}, \quad \delta = \frac{y}{b}, \quad W = \frac{w}{h}, \quad \tau = t\sqrt{\frac{Eh^3}{\rho a^4}}, \quad c = v_x\sqrt{\frac{\rho a^2}{Eh^3}}, \\ \varepsilon = \frac{a}{b}, \quad f = \frac{\Phi}{Eh^3}, \quad p = P\frac{a^4}{Eh^4}, \quad \omega = \varpi\sqrt{\frac{\rho a^4}{Eh^3}} \end{gathered} \tag{9}$$

Then the dimensionless form equations of the printing membrane under external excitation can be expressed as

$$\left(\frac{\partial^2 W}{\partial \tau^2} + 2c\frac{\partial^2 W}{\partial \varsigma \partial \tau} + c^2\frac{\partial^2 W}{\partial \varsigma^2}\right) - \varepsilon^2\frac{\partial^2 f}{\partial \delta^2}\frac{\partial^2 W}{\partial \varsigma^2} - \varepsilon^2\frac{\partial^2 f}{\partial \varsigma^2}\frac{\partial^2 W}{\partial \delta^2} = p\cos\omega\tau \tag{10}$$

$$\frac{\partial^4 f}{\partial \varsigma^4} + \varepsilon^4\frac{\partial^4 f}{\partial \delta^4} = \varepsilon^2\left(\frac{\partial^2 W}{\partial \varsigma \partial \delta}\right)^2 - \varepsilon^2\frac{\partial^2 W}{\partial \varsigma^2}\frac{\partial^2 W}{\partial \delta^2} \tag{11}$$

The boundary condition of nonlinear vibration equations of the moving membrane are

$$\varsigma = 0, 1 : \frac{\partial^2 f}{\partial \delta^2} = 1, \quad \frac{\partial^2 f}{\partial \varsigma \partial \delta} = 0, \quad W = 0 \tag{12}$$

$$\eta = 0, 1 : \frac{\partial^2 f}{\partial \varsigma^2} = 1, \quad \frac{\partial^2 f}{\partial \varsigma \partial \delta} = 0, \quad W = 0 \tag{13}$$

The state equation of the system

Suppose the solutions which satisfy the boundary conditions of equations (12) and (13) are

$$W(\varsigma, \delta, \tau) = U(\varsigma, \delta)q(\tau) \tag{14}$$

$$f(\varsigma, \delta, \tau) = F(\varsigma, \delta)q^2(\tau) \tag{15}$$

The displacement function satisfying the boundary condition is

$$U(\varsigma,\delta)=\sin\pi\varsigma\sin\pi\delta \tag{16}$$

Then substituting equation (16) into equation (11) yields

$$\frac{\partial^4 F}{\partial\varsigma^4}+\varepsilon^4\frac{\partial^4 F}{\partial\delta^4}=\frac{\varepsilon^2\pi^4}{2}(\cos2\pi\varsigma+\cos2\pi\delta) \tag{17}$$

The solution of the equation (17) is

$$F(\varsigma,\delta)=\frac{\varepsilon^2}{32}\cos2\pi\varsigma+\frac{1}{32\varepsilon^2}\cos2\pi\delta \tag{18}$$

Substituting equations (14) – (18) into equation (10) yields the following equation by using the Galerkin's method.

$$\iint_s\left\{U\frac{\partial^2 q(\tau)}{\partial\tau^2}+2c\frac{\partial U}{\partial\varsigma}\frac{\partial q(\tau)}{\partial\tau}+c^2\frac{\partial^2 U}{\partial\varsigma^2}q(\tau)-\varepsilon^2\frac{\partial^2 F}{\partial\delta^2}\frac{\partial^2 U}{\partial\varsigma^2}q^3(\tau)-\varepsilon^2\frac{\partial^2 F}{\partial\varsigma^2}\frac{\partial^2 U}{\partial\delta^2}q^3(\tau)-p\cos\omega\tau\right\}U(\varsigma,\delta)\mathrm{d}s=0 \tag{19}$$

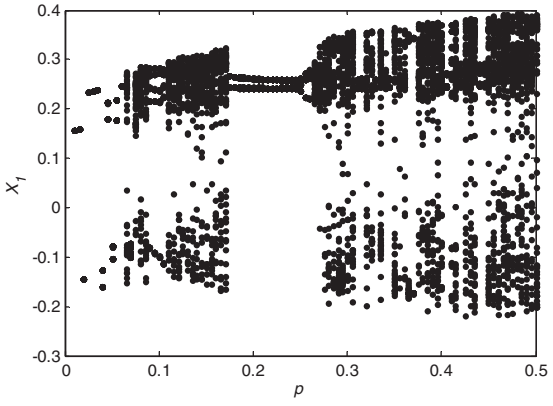

Figure 2. The amplitude of external excitation and displacement bifurcation diagram ($\omega=1$, $\gamma=0.1$, $\varepsilon=2$, and $c=0.5$).

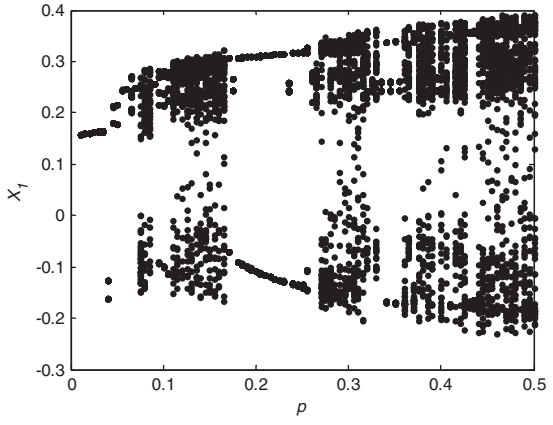

Figure 3. The amplitude of external excitation and displacement bifurcation diagram ($\omega=1$, $\gamma=0.1$, $\varepsilon=2$, $c=0.5$, the initial value is [0.1,0.1]).

The state equation of the moving printing membrane system under external excitation can be defined as

$$M\ddot{q} + B\dot{q} + Kq + Dq^3 = Q\cos\omega\tau \tag{20}$$

where

$$M = \iint_s U^2 \mathrm{d}s = \frac{1}{4} \tag{21}$$

$$B = 2c\iint_s \left(\frac{\partial U}{\partial \varsigma}\right) U\mathrm{d}s = 0 \tag{22}$$

$$K = c^2 \iint_s \frac{\partial^2 U}{\partial \varsigma^2} U\mathrm{d}s = -\frac{\pi^2 c^2}{4} \tag{23}$$

$$D = -\varepsilon^2 \iint_s \left(\frac{\partial^2 F}{\partial \delta^2}\frac{\partial^2 U}{\partial \varsigma^2} + \frac{\partial^2 F}{\partial \varsigma^2}\frac{\partial^2 U}{\partial \delta^2}\right) U\mathrm{d}s = \frac{\pi^4}{64}(1+\varepsilon^4) \tag{24}$$

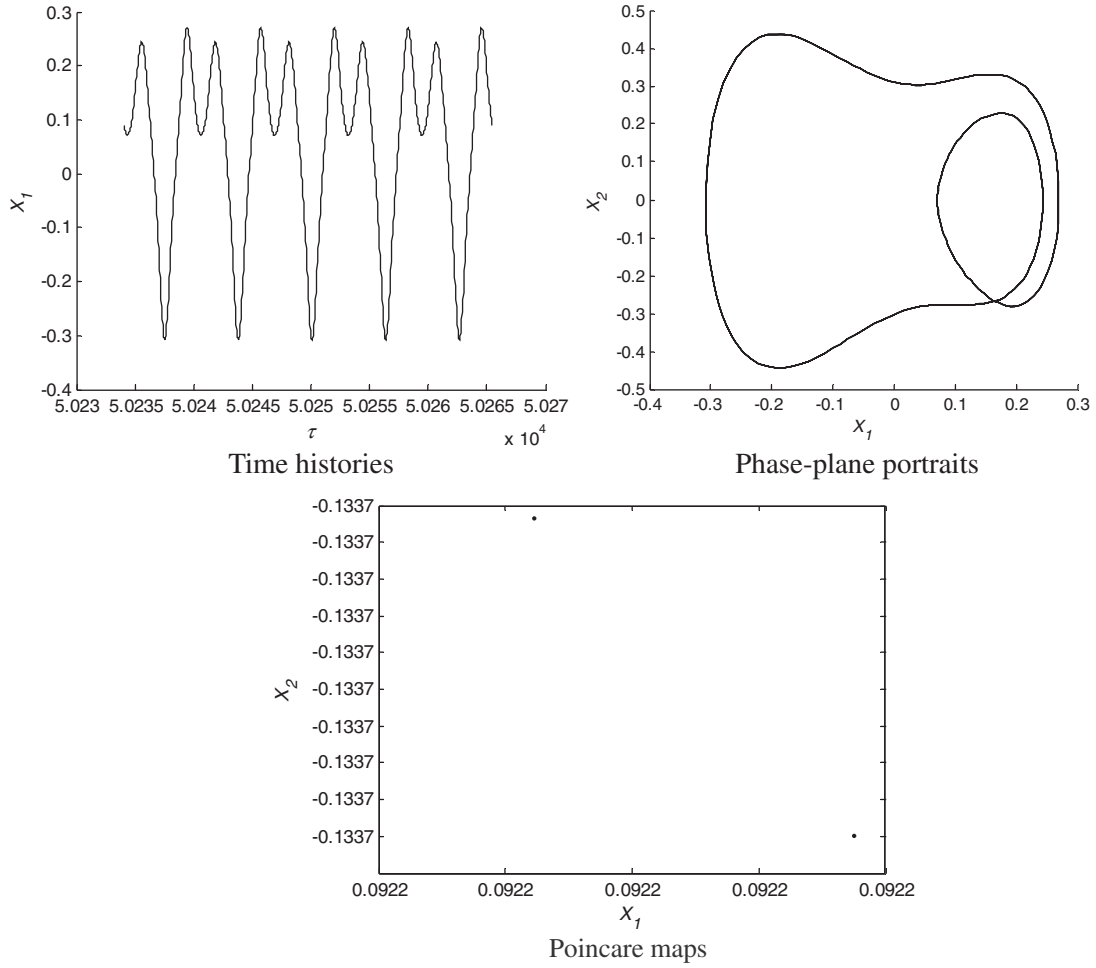

Figure 4. Time histories, phase-plane portraits and Poincare maps ($\omega = 1$, $\gamma = 0.1$, $c = 0.5$, $\varepsilon = 2$, and $p = 0.17$).

$$Q = p\iint_s U\mathrm{d}s = \frac{4}{\pi^2}p \tag{25}$$

The equation (20) can be written as

$$\ddot{q} - \pi^2 c^2 q + \frac{\pi^4}{16}\left(1+\varepsilon^4\right)q^3 = \frac{16}{\pi^2}p\cos\omega\tau \tag{26}$$

Consider the effect of damping, introducing the following parameter variables

$$X_1 = q, \quad X_2 = \dot{X}_1 \tag{27}$$

The equation (26) becomes

$$\dot{X}_2 = -\gamma X_2 + \pi^2 c^2 X_1 - \frac{\pi^4}{16}\left(1+\varepsilon^4\right){X_1}^3 + \frac{16}{\pi^2}p\cos\omega\tau \tag{28}$$

where γ is dimensionless damping coefficient.

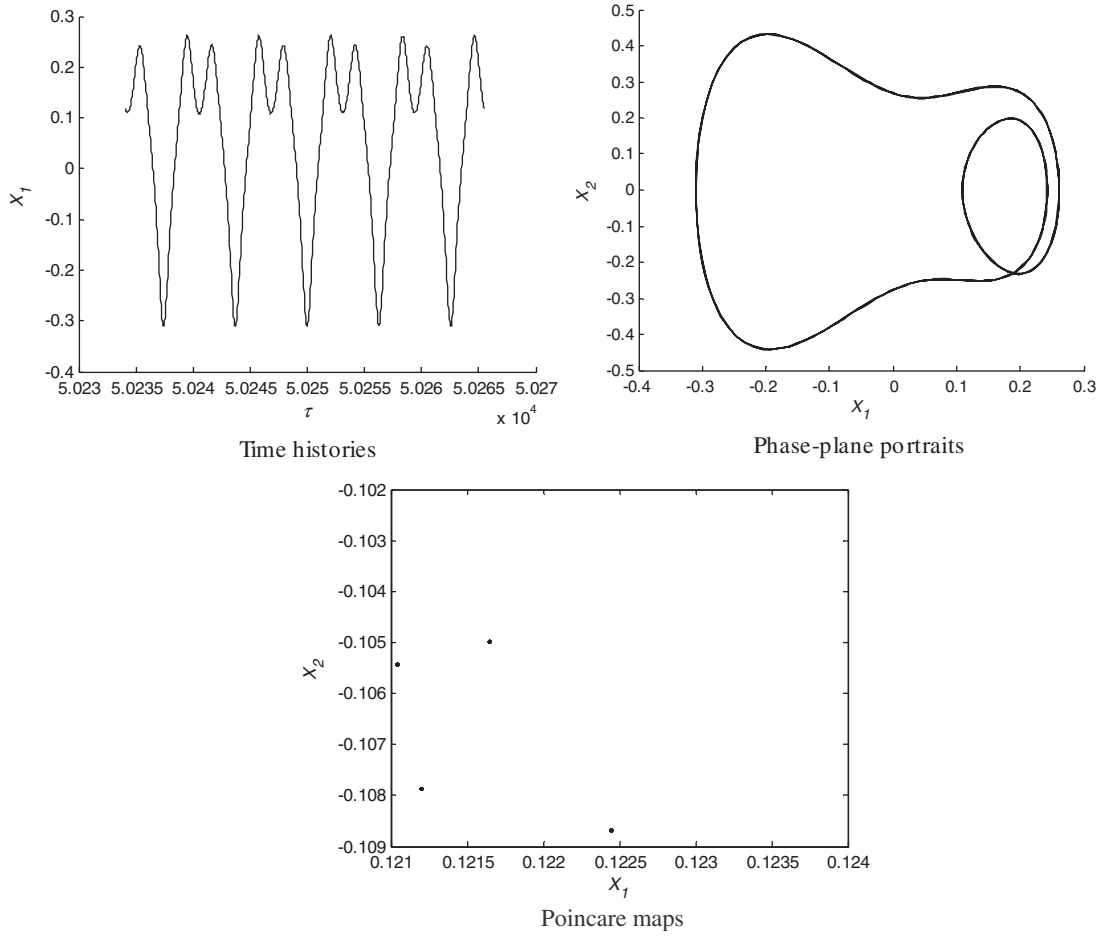

Figure 5. Time histories, phase-plane portraits and Poincare maps ($\omega = 1$, $\gamma = 0.1$, $c = 0.5$, $\varepsilon = 2$, and $p = 0.2$).

Numerical calculation and analysis

The state equation of the moving membrane system is numerically solved by using the fourth-order Runge–Kutta method. The effect of the amplitude of external excitation, aspect ratio, and damping coefficient of a membrane on the stability of the system are analyzed. The time histories, phase-plane portraits, Poincare maps, and bifurcation diagrams are applied to reveal the complex nonlinear dynamics of the system.

Influence of amplitude of external excitation on nonlinear vibration characteristics

Figure 2 shows the bifurcation diagram of dimensionless amplitude of external excitation and displacement when the dimensionless excitation frequency $\omega = 1$, the dimensionless damping coefficient $\gamma = 0.1$, the dimensionless velocity $c = 0.5$, the aspect ratio $\varepsilon = 2$, the initial value is [0.01,0], and the range of amplitude of external excitation is $0.01 \leq p \leq 0.5$. Figure 2 shows that when $0.01 \leq p < 0.065$, $0.085 < p < 0.11$, $0.17 < p < 0.264$, $0.305 < p < 0.32$, $0.36 < p < 0.375$, and $0.4 < p < 0.42$, the bifurcation diagram corresponds to a few points, indicating that the membrane is in a periodic motion state in these regions. When $0.065 < p < 0.085$, $0.11 < p < 0.17$, $0.264 < p < 0.305$, $0.32 < p < 0.36$, $0.375 < p < 0.4$, and $0.42 < p \leq 0.5$, the bifurcation diagram is a pile of dense points, indicating that the membrane is in chaotic state. To sum up, the system undergoes periodic motion to chaotic motion and then from chaotic motion to reciprocating changes in periodic motion. The bifurcation points are $p = 0.085$, $p = 0.17$, $p = 0.305$, $p = 0.36$, and $p = 0.4$. On the whole, the system has gone through two kinds of roads leading to chaos, period-doubling bifurcation into chaos and bursts of chaos.

Figure 3 shows the bifurcation diagram of amplitude of external excitation and displacement when the dimensionless excitation frequency $\omega = 1$, the dimensionless damping coefficient $\gamma = 0.1$, the dimensionless velocity $c = 0.5$, the aspect ratio $\varepsilon = 2$, the initial value is [0.1,0.1], and the range of amplitude of external excitation is $0.01 \leq p \leq 0.5$. As can be seen from Figures 2 and 3, the system motion process is significantly different due to the

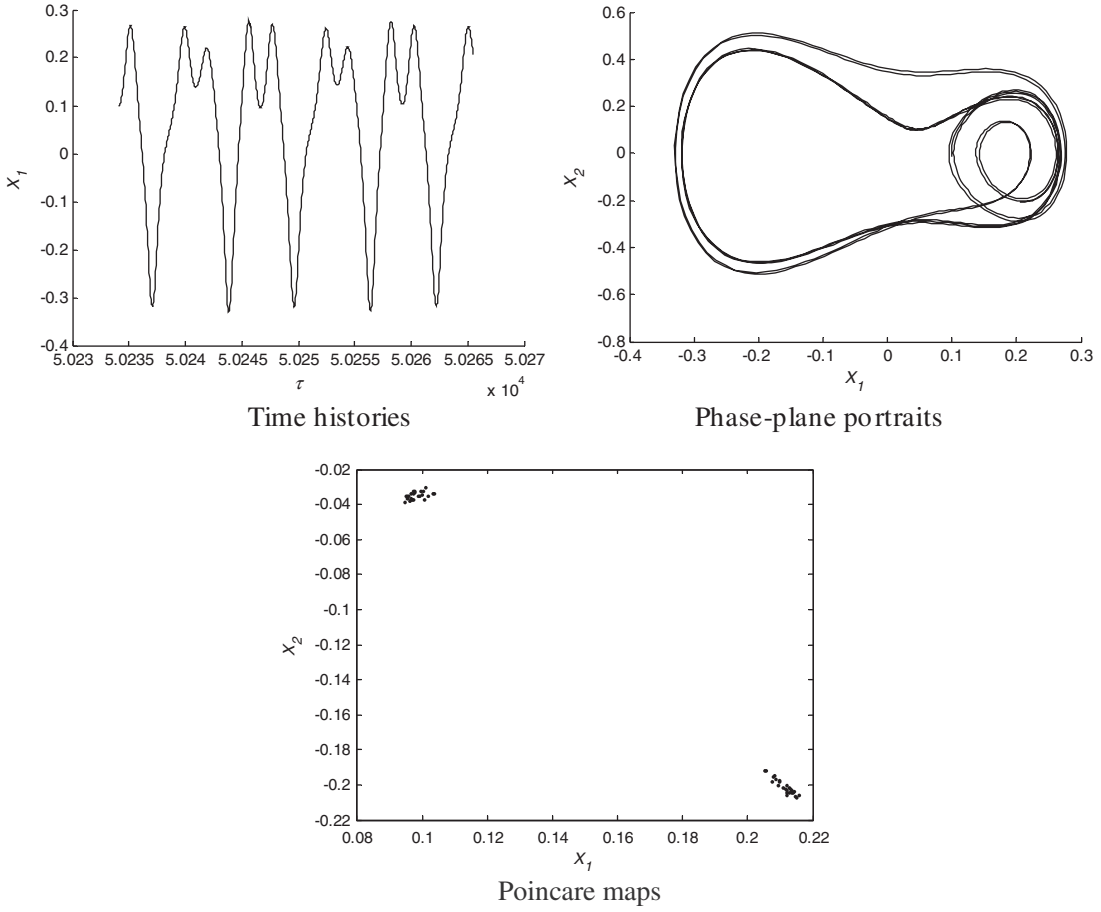

Figure 6. Time histories, phase-plane portraits and Poincare maps ($\omega = 1$, $\gamma = 0.1$, $c = 0.5$, $\varepsilon = 2$, and $p = 0.26$).

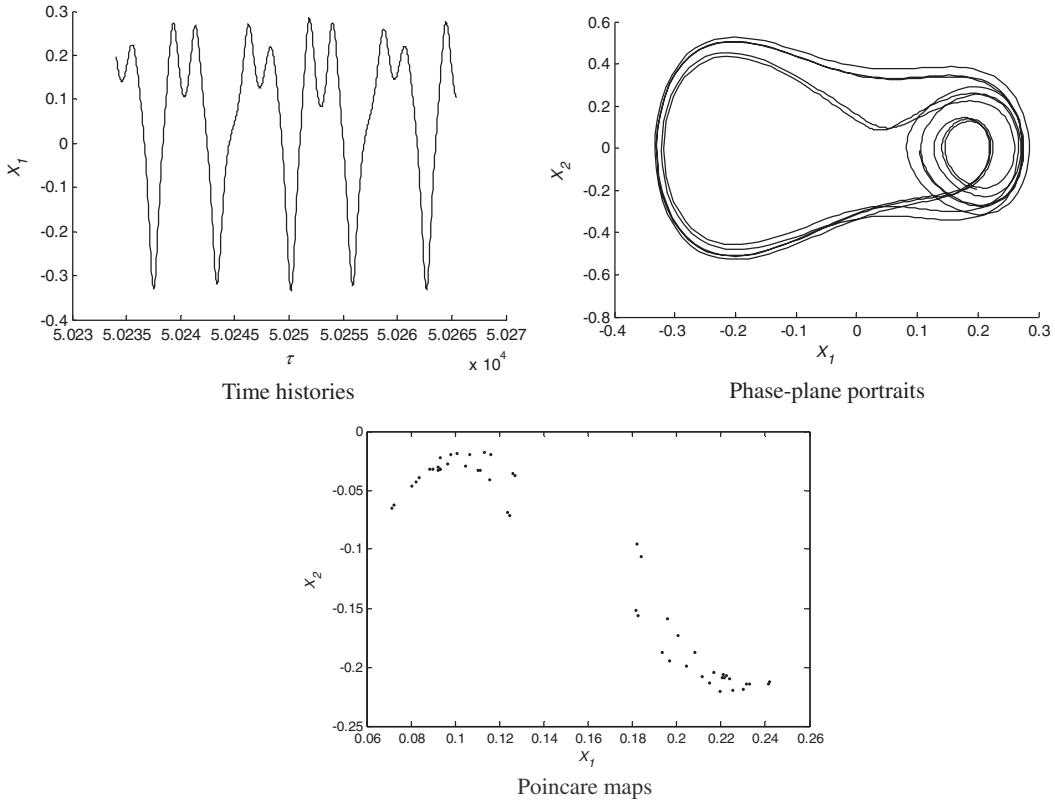

Figure 7. Time histories, phase-plane portraits and Poincare maps ($\omega = 1$, $\gamma = 0.1$, $c = 0.5$, $\varepsilon = 2$, and $p = 0.264$).

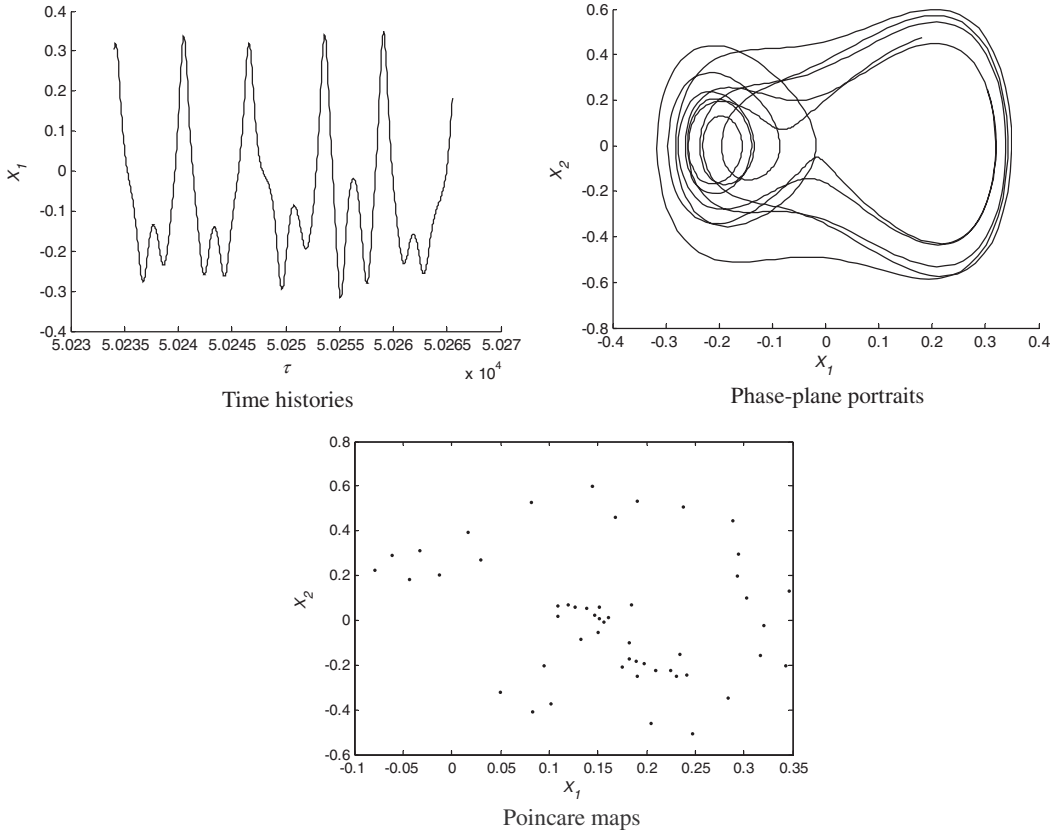

Figure 8. Time histories, phase-plane portraits and Poincare maps ($\omega = 1$, $\gamma = 0.1$, $c = 0.5$, $\varepsilon = 2$, and $p = 0.3$).

different initial values. Indicating that the nonlinear vibration of the membrane is sensitive to the initial conditions.

The membrane has a cycle of period-doubling bifurcation leading to chaos when $0.17 \leq p \leq 0.3$. To illustrate this bifurcation process, Figures 4–8 show time histories, phase-plane portraits, and Poincare maps when the amplitude of dimensionless external excitation is different.

Figures 4–8 show time histories, phase-plane portraits, and Poincare maps when $p = 0.17$, $p = 0.2$, $p = 0.26$, $p = 0.264$, and $p = 0.3$, respectively. When $p = 0.17$, the phase trajectory curve is regular closed graphic, and the Poincare section has two fixed points, which shows that the system is in double periodic motion state.

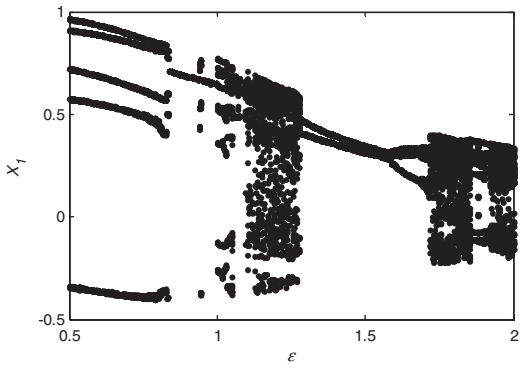

Figure 9. The aspect ratio and displacement bifurcation diagram ($\omega = 1$, $\gamma = 0.1$, $c = 0.3$, and $p = 0.4$).

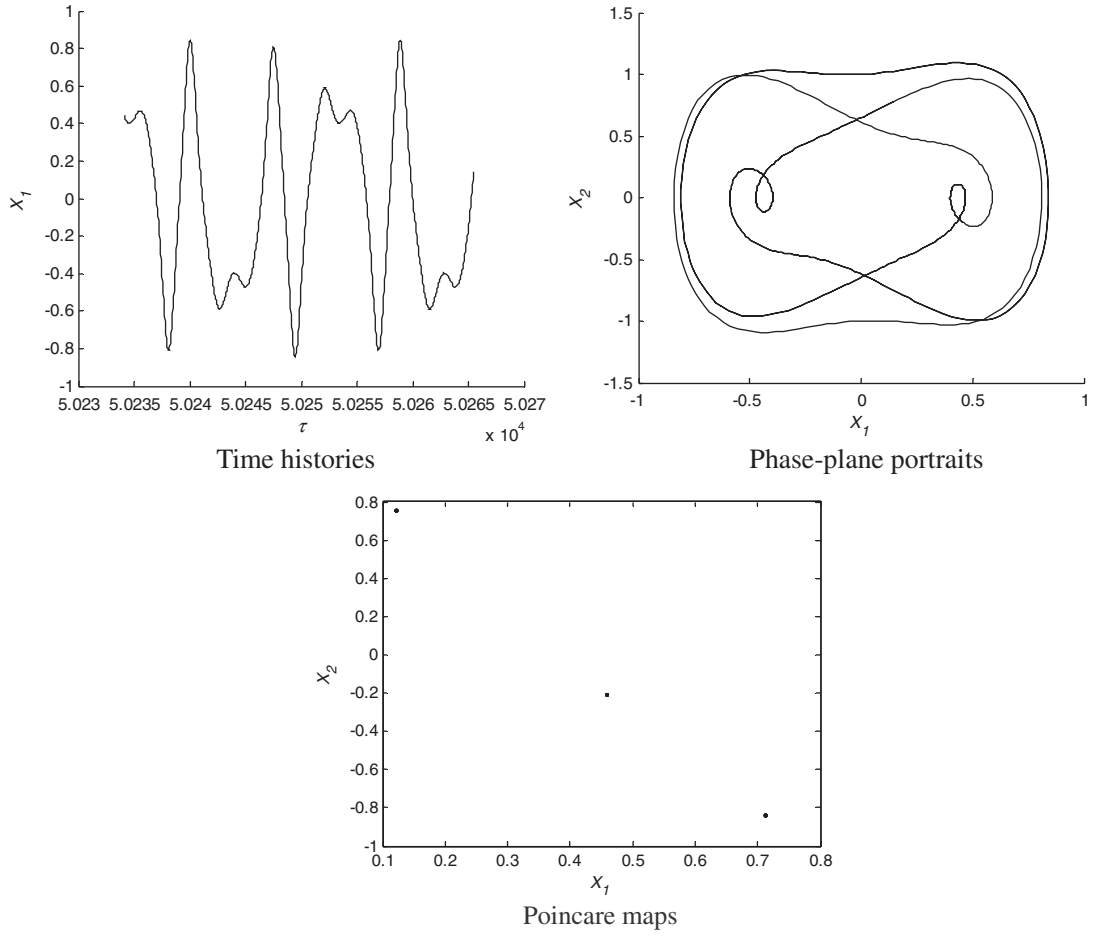

Figure 10. Time histories, phase-plane portraits and Poincare maps ($\omega = 1$, $\gamma = 0.1$, $c = 0.3$, $p = 0.4$, and $\varepsilon = 0.8$).

When $p = 0.2$, the phase trajectory curve is regular closed graphic, and the Poincare section has four fixed points, indicating that the system is in quadruple periodic motion state. When $p = 0.26$, the phase trajectory curve has a lot of regular closed graphics, and the Poincare section has a few discrete points, which indicates that the system is in the multiple periodic motion state. When $p = 0.264$ and $p = 0.3$, the phase trajectory curve is not closed curves, Poincare section has many dense points, indicating that the system is in chaotic motion state. To sum up, as the amplitude of dimensionless external excitation increases gradually, the system moves from double periodic motion to quadruple periodic motion, then to multiple periodic motion, and then enters chaotic motion. It can be seen that this way of generating chaos belongs to period-doubling bifurcation into chaos.

Influence of aspect ratio on nonlinear vibration characteristics

Figure 9 shows the bifurcation diagram of aspect ratio and dimensionless displacement when the dimensionless excitation frequency $\omega = 1$, the dimensionless damping coefficient $\gamma = 0.1$, the dimensionless velocity $c = 0.3$, the amplitude of dimensionless external excitation $p = 0.4$, the initial value is [0.01,0], and the range of aspect ratio is $0.5 \leq \varepsilon \leq 2$. The Figure 2 shows that when $0.5 \leq \varepsilon < 1.12$, $1.275 < \varepsilon < 1.715$, and $1.85 < \varepsilon < 1.92$, the bifurcation diagram corresponds to a few points, indicating that the membrane is in a periodic motion state in these regions, so the membrane is in a stable working range. When $1.12 < \varepsilon < 1.275$, $1.715 < \varepsilon < 1.85$, and $1.92 < \varepsilon \leq 2$, the bifurcation diagram has many dense points, indicating that the membrane is in chaotic state. So at these regions, the nonlinear vibration phenomenon is obvious, and the membrane is divergent instability. To sum up, with the increase in the dimensionless aspect ratio, the membrane suddenly fluctuates periodically and chaos and jumps randomly between the two. As the dimensionless aspect ratio increases, the burst phenomenon becomes more and more frequent. The periodic movement almost completely disappeared, and finally the system completely into the chaotic state. The bifurcation points are $\varepsilon = 1.275$, $\varepsilon = 1.57$, and $\varepsilon = 1.685$. We should make a reasonable choice

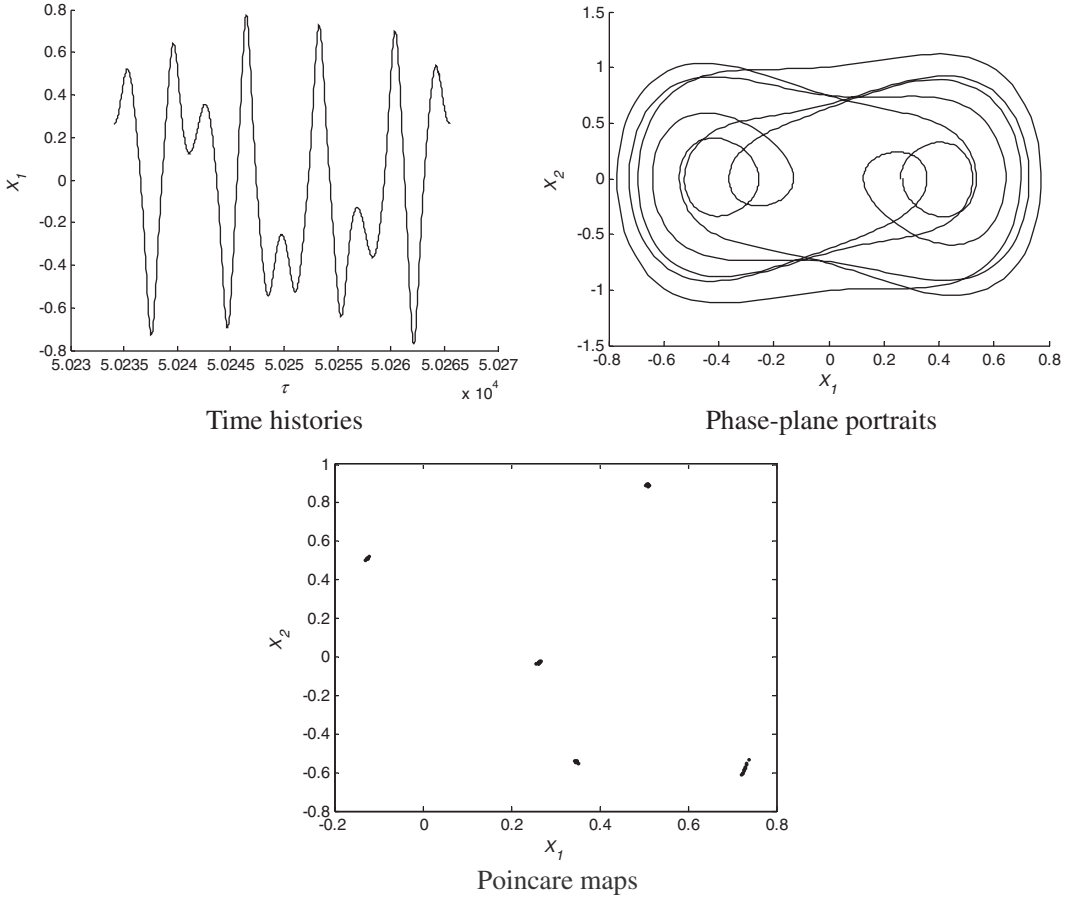

Figure 11. Time histories, phase-plane portraits and Poincare maps ($\omega = 1$, $\gamma = 0.1$, $c = 0.3$, $p = 0.4$, and $\varepsilon = 1$).

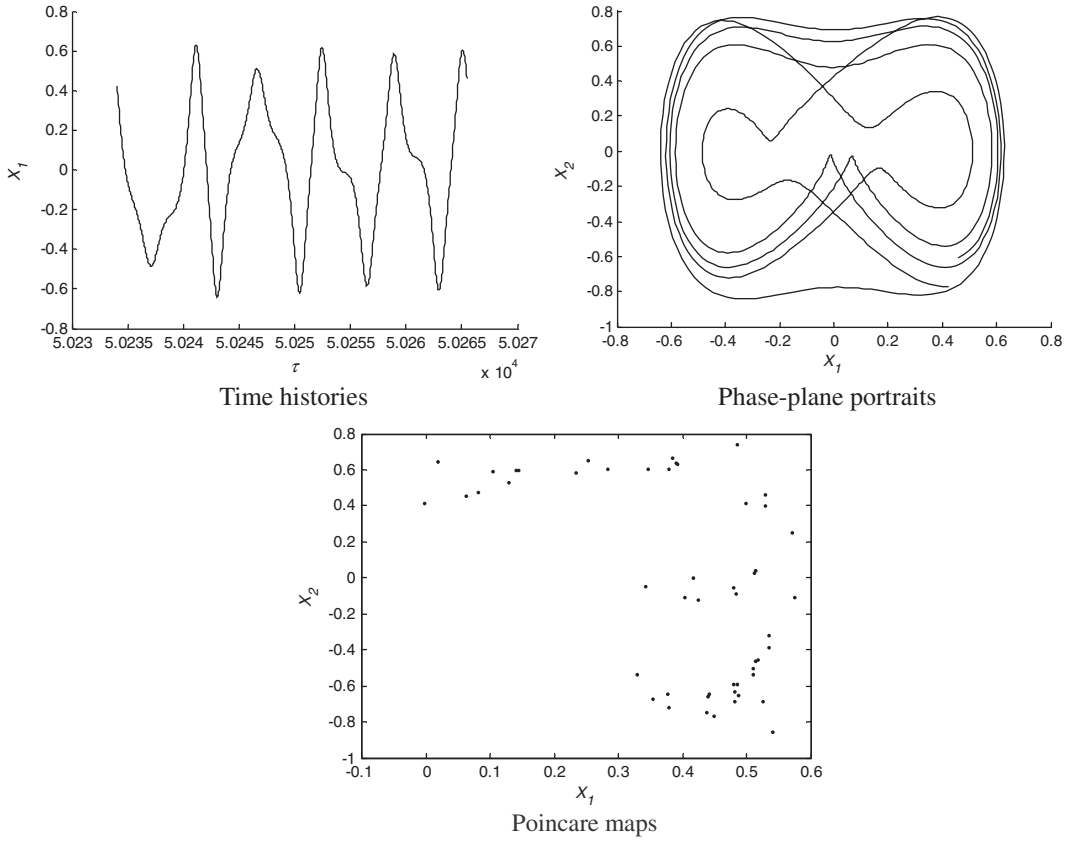

Figure 12. Time histories, phase-plane portraits and Poincare maps ($\omega = 1$, $\gamma = 0.1$, $c = 0.3$, $p = 0.4$, and $\varepsilon = 1.12$).

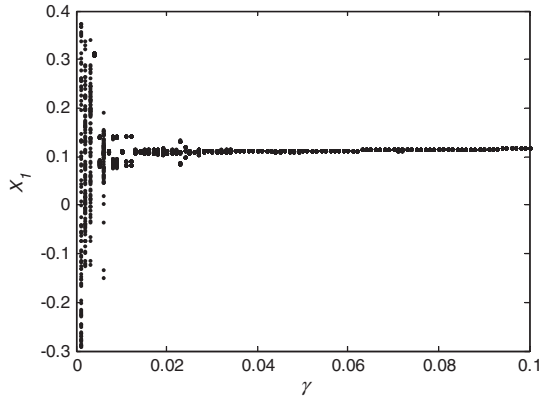

Figure 13. The damping coefficient and displacement bifurcation diagram ($\omega = 1$, $p = 0.2$, $\varepsilon = 2$, and $c = 0.5$).

of membrane aspect ratio to avoid the occurrence of chaos according to the printing requirements and improve the quality and accuracy of printing materials.

The membrane has a cycle of period-doubling bifurcation leading to chaos when $0.8 \leq \varepsilon \leq 1.12$. To illustrate this bifurcation process, Figures 10–12 show time histories, phase-plane portraits, and Poincare maps when the aspect ratio is different.

Figures 10–12 show time histories, phase-plane portraits, and Poincare maps when $\varepsilon = 0.8$, $\varepsilon = 1$, and $\varepsilon = 1.12$, respectively. When $\varepsilon = 0.8$, the phase trajectory curve is regular closed graphic, and the Poincare section has three fixed points, which shows that the system is in triple periodic motion state. When $\varepsilon = 1$, the phase trajectory curve has a lot of regular closed graphics, and the Poincare section has a few discrete points, which indicates that the system is in multiple periodic motion state. When $\varepsilon = 1.12$, the phase trajectory curve is not closed curves,

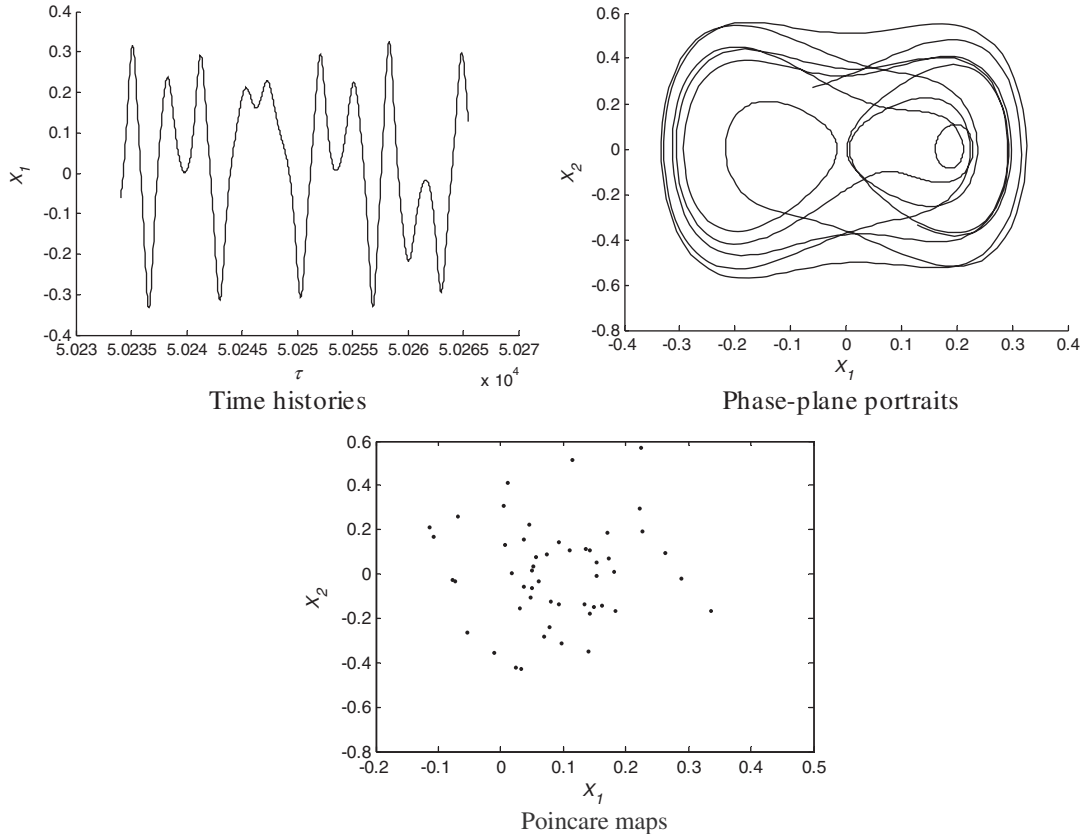

Figure 14. Time histories, phase-plane portraits and Poincare maps ($\omega = 1$, $\varepsilon = 2$, $c = 0.5$, $p = 0.2$, and $\gamma = 0.003$).

Poincare section has many dense points, indicating that the system is in chaotic motion state. To sum up, when $0.8 \leq \varepsilon \leq 1.12$, as the aspect ratio ε increases, the system undergoes triple periodic motion to the multiple periodic motion and then to the chaotic motion.

Influence of damping coefficient on nonlinear vibration characteristics

Figure 13 shows the bifurcation diagram of dimensionless damping coefficient and dimensionless displacement when the dimensionless excitation frequency $\omega = 1$, the aspect ratio $\varepsilon = 2$, the dimensionless velocity $c = 0.5$, the amplitude of dimensionless external excitation $p = 0.2$, the initial value is [0.001,0], and the range of damping coefficient is $0.001 \leq \gamma \leq 0.1$. The Figure 13 shows that when $0.001 \leq \gamma \leq 0.003$ and $\gamma = 0.006$, the bifurcation diagram has many dense points, indicating that the membrane is in chaotic state. So at these regions, the nonlinear vibration phenomenon is obvious, and the membrane is divergent instability. When $0.003 < \gamma < 0.006$ and $0.006 < \gamma \leq 0.1$, the bifurcation diagram corresponds to a few points, indicating that the membrane is in a periodic motion state in these regions, so the membrane is in a stable working range. To sum up, with the increase in the dimensionless damping coefficient, the system experiences chaotic motion to periodic motion, and then moves from periodic motion to chaos, finally entering the process of periodic motion completely.

Figure 14 shows time histories, phase-plane portraits, and Poincare maps when $\gamma = 0.003$, the phase trajectory curve is not closed curves, Poincare section has many dense points, indicating that the system is in chaotic motion state.

Conclusions

The nonlinear vibration characteristics of an axially moving printing membrane under external excitation are studied by using the fourth-order Runge–Kutta method. The influence of the amplitude of external excitation, aspect ratio, and damping coefficient of the printing membrane on the nonlinear vibration characteristics are

highlighted by using the time histories, phase-plane portraits, Poincare maps, and bifurcation diagrams. The conclusions are as follows:

1. When the dimensionless excitation frequency $\omega = 1$, the dimensionless damping coefficient $\gamma = 0.1$, the dimensionless velocity $c = 0.5$, the aspect ratio $\varepsilon = 2$, the initial value is [0.01,0], and the range of amplitude of the external excitation is $0.01 \leq p \leq 0.5$. When $0.01 \leq p < 0.065$, $0.085 < p < 0.11$, $0.17 < p < 0.264$, $0.305 < p < 0.32$, $0.36 < p < 0.375$, and $0.4 < p < 0.42$, the membrane is in a stable state in these regions. When $0.065 < p < 0.085$, $0.11 < p < 0.17$, $0.264 < p < 0.305$, $0.32 < p < 0.36$, $0.375 < p < 0.4$, and $0.42 < p \leq 0.5$, the membrane is in chaotic regions, so the membrane is divergent instability. To sum up, the system undergoes a reciprocating alternation of periodic motion to chaotic motion. The bifurcation points are $p = 0.085$, $p = 0.17$, $p = 0.305$, $p = 0.36$, and $p = 0.4$. On the whole, the system has gone through two kinds of roads leading to chaos, period-doubling bifurcation into chaos and bursts of chaos.
2. When the initial values are changed, the system motion process is significantly different. Indicating that the nonlinear vibration of the membrane is sensitive to the initial conditions.
3. When the dimensionless excitation frequency $\omega = 1$, the dimensionless damping coefficient $\gamma = 0.1$, the dimensionless velocity $c = 0.3$, the amplitude of dimensionless external excitation $p = 0.4$, the initial value is [0.01,0], and the range of aspect ratio is $0.5 \leq \varepsilon \leq 2$. When $0.5 \leq \varepsilon < 1.12$, $1.275 < \varepsilon < 1.715$, and $1.85 < \varepsilon < 1.92$, the membrane is in a stable working state in these regions. When $1.12 < \varepsilon < 1.275$, $1.715 < \varepsilon < 1.85$, and $1.92 < \varepsilon \leq 2$, the membrane is in chaotic regions, the membrane is divergent instability. The bifurcation points are $\varepsilon = 1.275$, $\varepsilon = 1.57$, and $\varepsilon = 1.685$. Periodic motion and chaotic motion occur when aspect ratio ε increases. We should make a reasonable choice of membrane aspect ratio to avoid the occurrence of chaos according to the printing requirements and improve the quality and accuracy of printing materials.
4. The dimensionless damping coefficient has effect on the nonlinear vibration, when $0.001 \leq \gamma \leq 0.003$ and $\gamma = 0.006$, the membrane is in chaotic state, and the membrane is divergent instability. When $0.003 < \gamma < 0.006$ and $0.006 < \gamma \leq 0.1$, the membrane is in a periodic motion state, and the membrane is in a stable working range in these regions. With the increase in the dimensionless damping coefficient, the system experiences chaotic motion to periodic motion and then moves from periodic motion to chaos, finally entering the periodic motion.
5. Overall, the stable working regions and divergent instability regions are obtained in different parameters. We should make a reasonable choice of membrane parameters in the stable working regions to avoid potential stability issues due to strong nonlinear phenomena.

Declaration of conflicting interests

The author(s) declared no potential conflicts of interest with respect to the research, authorship, and/or publication of this article.

Funding

The author(s) disclosed receipt of the following financial support for the research, authorship, and/or publication of this article: The author gratefully acknowledges the support of the Ph.D. Innovation fund projects of Xi'an University of Technology (Fund No. 310–252071702) and the National Natural Science Foundation of China (No. 11272253 and No. 11202159).

ORCID iD

Mingyue Shao http://orcid.org/0000-0003-3889-1999

References

1. Chen LQ, Tang YQ and Zu JW. Nonlinear transverse vibration of axially accelerating strings with exact internal resonances and longitudinally varying tensions. *Nonlinear Dyn* 2014; 76: 1443–1468.
2. Kesimli A, Özkaya E and Bağdatli SM. Nonlinear vibrations of spring-supported axially moving string. *Nonlinear Dyn* 2015; 81: 1523–1534.
3. Lewandowski R, Wielentejczyk P. Nonlinear vibration of viscoelastic beams described using fractional order derivatives. *J Sound Vib* 2017; 399: 228–243.
4. Zenkour AM. Free vibration of a microbeam resting on Pasternaks foundation via the Green-Naghdi thermoelasticity theory without energy dissipation. *J Low Freq Noise Vib Active Contr* 2016; 35: 303–311.

5. Hadj Y, Ahmed MS and Mostafa DE. Superharmonic resonance of cross-ply laminates by the method of multiple scales. *J Comput Nonlinear Dynam* 2017; 12: 054503
6. Beni YT, Mehralian F and Zeverdejani MK. Free vibration of anisotropic single-walled carbon nanotube based on couple stress theory for different chirality. *J Low Freq Noise Vib Active Contr* 2017; 36: 277–293.
7. Liu C, Yue S and Zhou J. Piezoelectric optimal delayed feedback control for nonlinear vibration of beams. *J Low Freq Noise Vib Active Contr* 2016; 35: 25–38.
8. Hirwani CK, Panda SK and Mahapatra TR. Nonlinear finite element analysis of transient behavior of delaminated composite plate. *J Vib Acoust* 2018; 140: 021001
9. Kumar A, Singha MK and Tiwari V. Nonlinear bending and vibration analyses of quadrilateral composite plates. *Thin Wall Struct* 2017; 113: 170–180.
10. Chai YY, Li FM and Song ZG. Nonlinear vibration behaviors of composite laminated plates with time-dependent base excitation and boundary conditions. *Int J Nonlinear Sci Numer Simul* 2017; 18: 145–161.
11. Ghayesh MH, Amabili M and Païdoussis MP. Nonlinear dynamics of axially moving plates. *J Sound Vib* 2013; 332: 391–406.
12. Khanna A and Kaur N. Vibration of non-homogeneous plate subject to thermal gradient. *J Low Freq Noise Vib Active Contr* 2014; 33: 13–26.
13. Boz U, Aridogan U and Basdogan I. A numerical and experimental study of optimal velocity feedback control for vibration suppression of a plate-like structure. *J Low Freq Noise Vib Active Contr* 2015; 34: 343–360.
14. Hu Y and Hu P, ZJ. Strongly nonlinear subharmonic resonance and chaotic motion of axially moving thin plate in magnetic field. *J Comput Nonlinear Dynam* 2015; 10: 021010.
15. Ansari R, Shakouri AH, Bazdid-Vahdati M, et al. A non-classical finite element approach for the nonlinear analysis of micropolar plates. *J Comput Nonlinear Dynam* 2017; 12: 011019.
16. Saleema P and Manoranjan B. Large amplitude free flexural vibration of stiffened plates using superparametric element. *J Comput Nonlinear Dynam* 2016; 12: 031013.
17. Khanna A and Singhal A. Effect of plate's parameters on vibration of isotropic tapered rectangular plate with different boundary conditions. *J Low Freq Noise Vib Active Contr* 2016; 35: 149–151.
18. Wang YQ and Zu JW. Nonlinear dynamic thermoelastic response of rectangular FGM plates with longitudinal velocity. *Compos B Eng* 2017; 117: 74–88.
19. Lin CC and Mote CD. Equilibrium displacement and stress distribution in a two-dimensional, axially moving web under transverse loading. *J Appl Mech* 1995; 62: 772–779.
20. Koivurova H and Pramila A. Nonlinear vibration of axially moving membrane by finite element method. *Comput Mech* 1997; 20: 573–581.
21. Kulachenko A, Gradin P and Koivurova H. Modeling the dynamical behaviour of a paper web part I. *Comput Struct* 2007; 85: 131–147.
22. Kulachenko A, Gradin P and Koivurova H. Modelling the dynamical behaviour of a paper web. Part II. *Comput Struct* 2007; 85: 148–157.
23. Zhao FQ and Wang ZM. Nonlinear vibration analysis of a moving rectangular membrane (in Chinese). *Mech Sci Technol Aerosp Eng* 2010; 29: 768–771.
24. Soares RM and Gonçalves PB. Nonlinear vibrations and instabilities of a stretched hyperelastic annular membrane. *Int J Solid Struct* 2012; 49: 514–526.
25. Marynowski K. Non-linear vibrations of an axially moving viscoelastic web with time-dependent tension. *Chaos Solitons Fractals* 2004; 21: 481–490.
26. Luo ACJ. A theory for nonlinear soft webs. *Comm Nonlinear Sci Numer Simul* 2011; 16: 2184–2199.
27. Nguyen QC, Hong KS. Stabilization of an axially moving web via regulation of axial velocity. *J Sound Vib* 2011; 330: 4676–4688.
28. Banichuk N, Jeronen J, Neittaanmäki P, et al. Theoretical study on travelling web dynamics and instability under non-homogeneous tension. *Int J Mech Sci* 2013; 66: 132–140.
29. Wetherhold R and Padliya PS. Design aspects of nonlinear vibration analysis of rectangular orthotropic membranes. *J Vib Acoust* 2014; 136: 034506
30. Li D, Zheng ZL, Tian Y, et al. Stochastic nonlinear vibration and reliability of orthotropic membrane structure under impact load. *Thin Wall Struct* 2017; 119: 247–255.
31. Ma L, Chen J, Tang W, et al. Transverse vibration and instability of axially travelling web subjected to non-homogeneous tension. *Int J Mech Sci* 2017; 133: 752–758.
32. Xu ZL. *Elastic mechanics (Part II)*. Beijing: Higher Education Press, 2015, pp.142–146 (in Chinese).